FULL PAPER

Metalens Spectrometers

ADVANCED
OPTICAL
MATERIALS

www.advopticalmat.de

Compact Aberration-Corrected Spectrometers in the Visible Using Dispersion-Tailored Metasurfaces

Alexander Y. Zhu, Wei Ting Chen,* Jared Sisler, Kerolos M. A. Yousef, Eric Lee, Yao-Wei Huang, Cheng-Wei Qiu, and Federico Capasso*

The spectral resolution and range of conventional spectrometers are typically limited by optical aberrations of their focusing elements, mainly due to chromatically induced astigmatism and an intrinsically curved focal plane. Traditional approaches to overcome this challenge require additional optical components which introduce significant bulk and design complexity to the system and prevent easy integration with portable devices. Here a single planar off-axis focusing metalens consisting of subwavelength TiO$_2$ nanofins whose focal spots lie along a plane and undergo minimal focal spot broadening for almost 200 nm across the visible spectrum is demonstrated. This allows us to achieve a miniature aberration-corrected spectrometer with nanometer spectral resolution, while having a beam propagation distance of only 4 cm to the camera plane. This is achieved by dispersion engineering: tailoring the phase, group delay (GD) and GD dispersion of the metalens. This approach is general and can also be used to introduce customized functionalities to the metalens such as a linear dispersion in the frequency domain with minimal additional overhead.

1. Introduction

Spectrometers are essential tools for probing light–matter interactions and understanding a variety of phenomena such as Raman scattering or fluorescence. They are used extensively in numerous applications ranging from basic scientific research[1,2] to environmental monitoring,[3] food safety,[4] and disease diagnostics.[5,6]

A. Y. Zhu, Dr. W. T. Chen, J. Sisler, K. M. A. Yousef, E. Lee,
Dr. Y.-W. Huang, Prof. C.-W. Qiu, Prof. F. Capasso
Harvard John A. Paulson School of Engineering and Applied Sciences
Harvard University
Cambridge, MA 02138, USA
E-mail: weitingchen@seas.harvard.edu; capasso@seas.harvard.edu
J. Sisler, E. Lee
University of Waterloo
Waterloo, ON N2L 3G1, Canada
K. M. A. Yousef
College of Biotechnology
Misr University for Science and Technology
Giza 77, Egypt
Dr. Y.-W. Huang, Prof. C.-W. Qiu
National University of Singapore
Singapore 119077, Singapore

The key components of a spectrometer are a dispersive element, such as a grating, followed by a focusing lens. These are usually arranged in a Czerny–Turner configuration.[7] However, different wavelengths of incident light are focused along a curved surface as opposed to a planar one; as a result the focal spot broadens and becomes aberrated due to astigmatism and field curvature.[7] These factors result in a tradeoff between the spectral resolution, which is related to the size and quality of the focal spot, and the spectral range of the spectrometer.

Conventional methods to overcome this challenge involve additional optical components (e.g., multiple lenses) or precisely machined parts to correct for these aberrations, such as wedge-shaped cylindrical lenses,[8] toroidal gratings,[9] and freeform elements.[10] These are typically fabricated from aspheric blanks and introduce a significant overhead in terms of overall device cost and complexity. This also poses a significant challenge for truly compact, low-cost, handheld aberration-corrected spectrometers.

Recently, metasurfaces comprising of subwavelength scale nanostructures have received much attention from the research community.[11] They allow for exquisite control over the output wavefront of light,[12–15] and have been used to demonstrate ultracompact analogs of numerous optical components, such as lenses,[16–18] holograms,[19–21] and polarimeters.[22–24] An important advantage of metasurfaces is their ability to integrate multiple functionalities within a single planar device, thereby greatly reducing bulk and system complexity. For example, in an earlier work,[25] we demonstrated off-axis focusing metalenses capable of simultaneously focusing and dispersing light: they thus integrate the functionality of both the grating and the focusing lens in a single optical component. Additionally, by engineering the off-axis focusing angle very large dispersions can be obtained;[26] this allows one to achieve a miniature spectrometer with subnanometer resolution with a working distance of only a few centimeters from the lens to the detector. This distance is not fundamentally limited in any way; it is dependent on the desired specifications of the metalens, and in principle could even be much smaller, enabling monolithic integration with detectors.

However, these off-axis focusing metalenses face the same challenges as their refractive and diffractive counterparts[27–30]

**ADVANCED
SCIENCE NEWS**
www.advancedsciencenews.com

**ADVANCED
OPTICAL
MATERIALS**
www.advopticalmat.de

in terms of possessing an intrinsically curved focal plane and experiencing aberrations for wavelengths different from the design.[31] Here, we demonstrate an aberration-corrected off-axis metalens which maintains its focal spot profile across a broad bandwidth, by simultaneously engineering the phase and its higher order derivatives with respect to frequency (i.e., group delay (GD) and GD dispersion (GDD)). We characterize its focusing and dispersive behavior and demonstrate an ultra-compact spectrometer with a working distance of 4 cm and nanometer spectral resolution over approximately 200 nm bandwidth in the visible (spectral resolutions are 0.96, 1.01, 1.06, and 1.14 nm at 488, 532, 632, 660 nm incident wavelengths, respectively).

2. Off-Axis Metalenses

2.1. Design via Phase and Dispersion Engineering

Figure 1 shows the schematic images and scanning electron micrographs of such an aberration-corrected, off-axis metalens. It was fabricated via electron-beam lithography and atomic layer deposition of titanium oxide.[32] Its constituent unit cell (400×400 nm^2) comprises one or more rectangular nanofins of height 600 nm (Figure 1a,b). The gap between the nanofins is fixed at either 60 or 90 nm. Due to its form birefringence, each successive unit cell can be rotated to impart the desired phase using the geometric phase concept.[33,34] Additionally, multiple nanofins in close proximity within a unit cell behave analogously to coupled waveguides and can support electromagnetic modes with tunable dispersion.[17,35] Their optical properties are determined by varying the length (l) and

width (w) of the fins (Figure 1a). This choice of elements enables us to decouple the output phase of light from GD and its higher order derivatives, so that we can independently specify both a target phase profile as well as its behavior at wavelengths different from the design.

The off-axis metalens has dimensions of 800×250 μm with a focal length (f) of 4 cm and focusing angle (θ) of 25° at the design wavelength of 470 nm (Figure 1b). This acts as both the focusing and dispersive element in a traditional spectrometer since different wavelengths of light are focused at different spots along the plane of the detector, enabling one to obtain spectral information. This is schematically illustrated by the rainbow-colored bar in Figure 1b. Scanning electron micrographs of the fabricated device are shown in Figure 1c,d. Note that the metalens is essentially a rectangular cut from a circular metalens with a radial phase profile; as a result, phase gradients are present along both x and y directions. However, by design the primary focusing will be along the x-axis. The phase gradient imparted along y is therefore small, as evidenced by the small difference in rotation angles of the unit cells in the vertical direction (Figure 1c,d).

To achieve off-axis focusing, the phase profile of the metalens must satisfy:

$$\varphi(x,y,\omega) = -\frac{\omega}{c}\left(\sqrt{(x-x_f)^2 + y^2 + (z-z_f)^2} - f(\omega)\right) \tag{1}$$

where x and y are spatial coordinates along the lens (refer to coordinate system shown in Figure 1b), and ω is the angular frequency of incident light. c is the speed of light in vacuum. Equation (1) ensures that light from all regions of the metalens travels toward the focus and interferes constructively. The focal
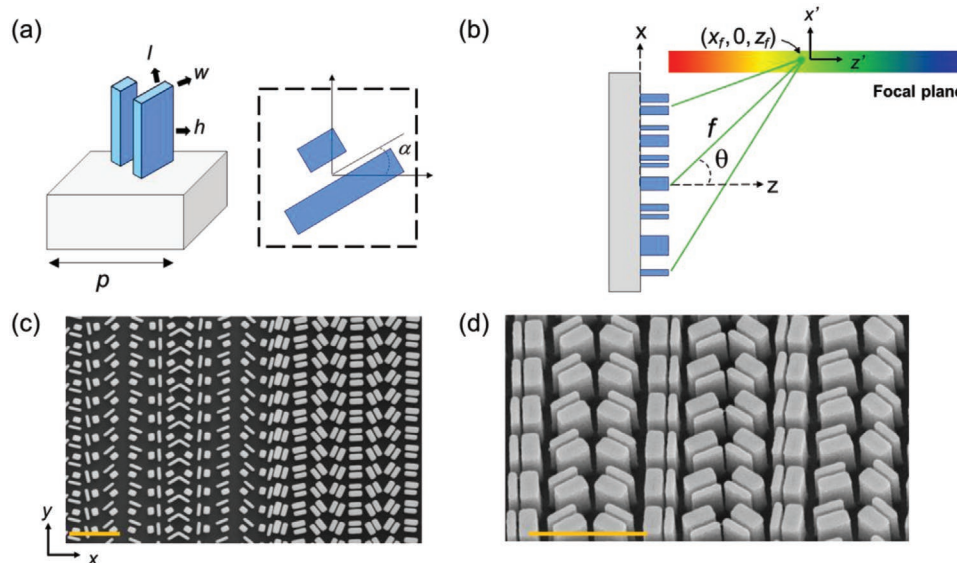

Figure 1. a) Schematic of a coupled nanofin structure with unit cell size p, and length, width, and height characterized by l, w, and h, respectively. The latter parameters are varied to obtain a library of elements with different dispersion properties. The entire unit cell can be rotated by an angle α to provide a phase shift of 2α for left-handed circularly polarized light, using the geometric phase principle. b) Schematic of an off-axis metalens comprising these coupled nano-fin structures. The focal spot is located at (x_f, 0, z_f). We also define a primed coordinate system centered on the focal spot. The rainbow-colored line indicates the flat focal plane of the lens for different wavelengths in the visible. c), d) Scanning electron micrographs of a fabricated aberration-corrected off-axis metalens. Note that the direction with the largest phase gradient is along the horizontal x-axis. Scale bars: 1 μm

length $f(\omega)$ and its corresponding spatial coordinates (x_f and z_f) are straightforwardly related to the focusing angle $\theta(\omega)$ by

$$x_f = f(\omega) \cdot \sin(\theta(\omega)) \tag{2}$$

$$z_f = f(\omega) \cdot \cos(\theta(\omega)) \tag{3}$$

We wish to tailor $f(\omega)$ such that all the focal spots for different wavelengths lie along a plane orthogonal to the x-axis and parallel to the z-axis. This choice makes alignment easier and prevents background light from reaching the detector. Thus, from Equation (2), the focal length at an arbitrary frequency ω must satisfy

$$f(\omega) \cdot \sin(\theta(\omega)) = f(\omega_d) \cdot \sin(\theta(\omega_d)) \tag{4}$$

where $f(\omega_d)$, ω_d, and $\theta(\omega_d)$ correspond to the focal length, angular frequency, and off-axis angle at the design wavelength $\lambda_d = 470$ nm, respectively. Equation (4) can be satisfied by designing the dispersion of focal length and focusing angle according to

$$f(\omega) = \frac{\omega}{\omega_d} f(\omega_d);$$
$$\sin(\theta(\omega)) = \frac{\omega_d}{\omega} \sin(\theta(\omega_d)) \tag{5}$$

This choice of focal plane ensures that minimal dispersion engineering is needed along the y-direction, so that the metalens can be scaled up to match the size of entrance slits of spectrometers in order to capture light more efficiently (see Figure S2, Supporting Information). Together, Equations (1)–(5) dictate the frequency-dependent phase profile of such an off-axis aberration-corrected metalens, which is noticeably different from prior metalens spectrometers.[25,26]

We can implement this phase profile by Taylor-expanding Equation (1) at the design angular frequency ω_d:

$$\varphi(x,y,\omega) = \varphi(x,y,\omega_d) + \frac{\partial \varphi}{\partial \omega} \cdot (\omega - \omega_d) + \frac{\partial^2 \varphi}{2\partial \omega^2} \cdot (\omega - \omega_d)^2 \ldots \tag{6}$$

The partial derivative in the second term $\left(\frac{\partial \varphi}{\partial \omega}\right)$ is the GD; the next higher order term $\left(\frac{\partial^2 \varphi}{\partial \omega^2}\right)$ is referred to as the GDD. As discussed earlier, by appropriate choice of parameters for the coupled nanofins within a unit cell, one can separately implement both the desired phase and GD/GDD profiles. Note that these quantities are spatially dependent, and they are relative values defined with respect to the nanostructure at the center of the metalens.

Figure 2 compares the simulated results of an off-axis metalens designed using the procedure described above to that of a traditional Berry phase lens[16] where only the phase profile (zeroth-order derivative term in Equation (6)) is implemented. The Berry phase lens represents a control sample for the case without dispersion engineering and performs similarly to an off-axis focusing Fresnel lens.[27] Both lenses have the same dimensions and specifications. From the ray-tracing results in Figure 2a,b (calculated using Zemax OpticStudio),

one observes that the Berry phase lens focuses along a curved surface while the aberration-corrected metalens focuses along a plane orthogonal to the x-axis, accurately fulfilling the design based on Equation (1). The latter thus avoids the problem of focal spot broadening due to projection on a planar surface, such as a camera. It is important to note that by implementing the GD and GDD terms in Equation (6), one also corrects for the wavelength dependent aberrations, such as astigmatism, of the Berry phase lens. Astigmatism occurs in this case due to different foci of sagittal and tangential rays (incident rays passing through the x- and y-axes of the lens, respectively) as incident wavelengths deviate from the design. In an off-axis configuration, changes in incident wavelength will result in unequal shifts of the sagittal and tangential focal planes and contribute to an asymmetric broadening of the focal spot. This is observed in Figure 2c, as the focal spots at wavelengths away from the design wavelength of 470 nm rapidly broaden and become aberrated along the z'-direction. Consequently, they are no longer diffraction limited beyond 530 nm, which would severely limit the spectral range of a system using the Berry phase lens. In contrast, using our current approach (i.e., the aberration-corrected metalens) the phase profile remains close to the ideal requirement at multiple different wavelengths due to the presence of the dispersion terms. As a result, we can achieve diffraction-limited focusing across the entire visible spectrum (Figure 2d) while staying true to a single layer metasurface design, without the use of additional correcting optics.

2.2. Experimental Characterization

Next we experimentally characterized the performance of our metalens, again using a traditional Berry phase lens as a control. The results are shown in **Figure 3**. We illuminated each lens with collimated monochromatic laser light at 488, 532, 632, and 660 nm, and captured the resulting focal spots with a CMOS camera (Thorlabs DCC 1545M) situated along the z'-axis. We observe that the focal spots of the aberration-corrected metalens remain well defined with a single peak for all four wavelengths across the visible (Figure 3a–d), with a hint of broadening and asymmetry around 660 nm. In contrast, the focal spots of the Berry phase lens become significantly aberrated beyond 532 nm wavelength, with strong side-lobes appearing which would severely degrade the overall spectral resolution of the system. These results agree well with simulations (see Figure S2, Supporting Information). We note that close to the design wavelength (i.e., at 488 nm), the Berry phase lens has a higher quality focal spot with a slightly narrower full-width-at-half-maximum (FWHM). We attribute this to fabrication errors and coupling effects between neighboring unit cells in the aberration-corrected metalens since the structures are brought within closer proximity (compared to a single nanofin in the Berry phase lens) as they are rotated, thereby perturbing the optical modes and causing additional phase or dispersion variation not initially accounted for during the design. However, this can be mitigated by expanding the range of parameters of the simulation library in the design step. Furthermore, the difference in FWHM of the focal spots at 488 nm is only about 6 µm, which is approximately the size of one camera pixel (5.2 µm).
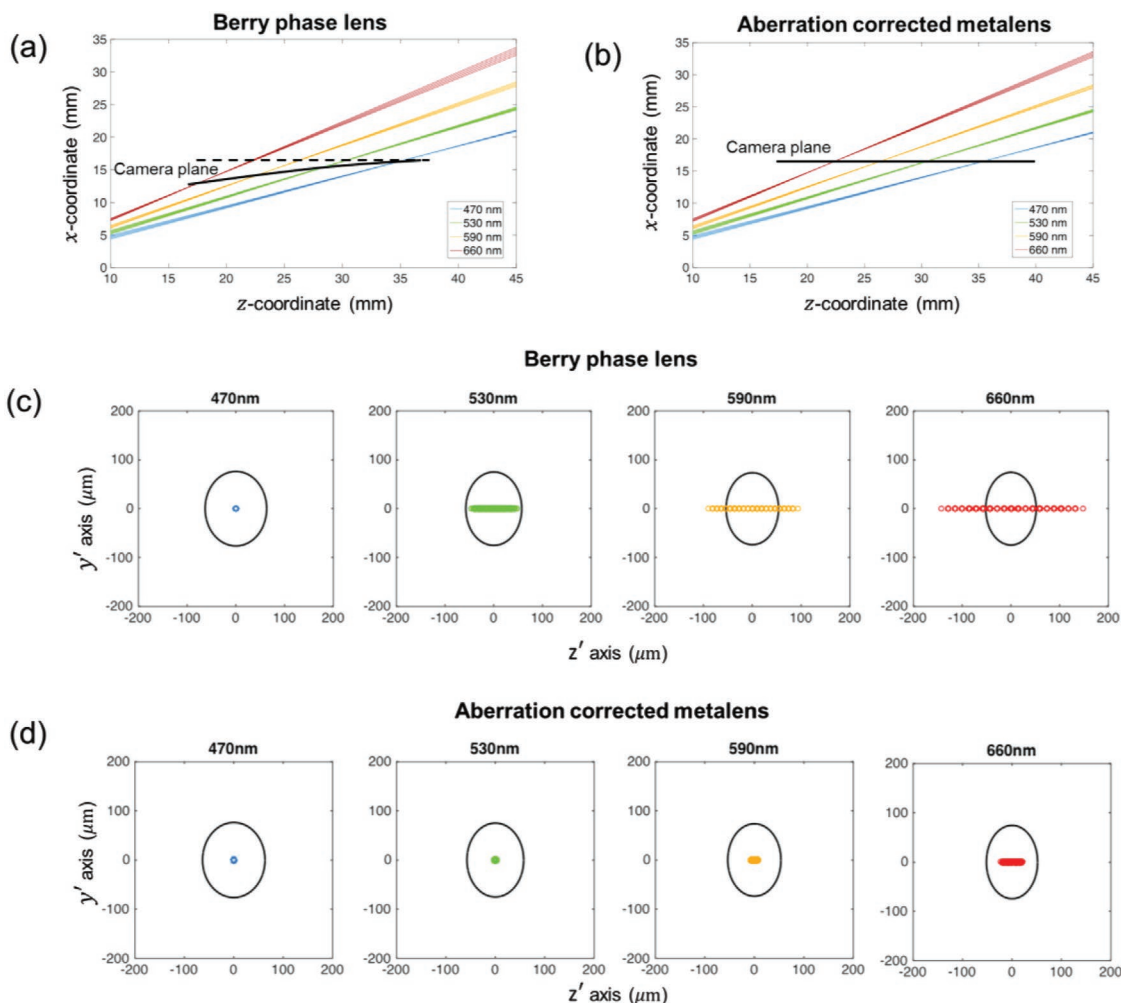
Figure 2. Ray-tracing simulations of a) a regular Berry-phase lens and b) the aberration-corrected metalens. The metalenses were designed with focal length $f = 40$ mm and focusing angle $\alpha = 25$ degrees at wavelength $\lambda = 470$ nm. The focusing planes for each case are indicated by bold lines; the dashed line in a) is horizontal and meant as a reference to the curved focal plane. c) Diagrams of the focal spots at their respective focal planes calculated from ray-tracing for the Berry phase lens and d) aberration-corrected metalens, respectively, under wavelengths of 470, 530, 590, and 660 nm illumination. The oval outline represents the diffraction-limited focal spot size; it is oval due to the rectangular dimensions of the metalens. Labeling of the coordinates follows the scheme shown in Figure 1b. The asymmetric broadening of the focal spot along the z'-axis is due to astigmatism as the incident wavelength changes.

We subsequently characterized the dispersion and efficiency of the aberration-corrected metalens, as shown in **Figure 4** These properties were measured using a collimated supercontinuum laser source (SuperK Varia, NKT Photonics), with wavelengths ranging from 450 to 700 nm in steps of 5 nm. To obtain the dispersion, at each wavelength the focal spot position was captured using our camera and the shift in spatial position (compared to the focal spot at the previous wavelength) was recorded; the results are plotted in Figure 4a. We obtain a reciprocal linear dispersion ($\Delta\lambda/\Delta r$) of 0.013 nm µm^{-1}; this translates into an intrinsic spectral resolution of 0.77 nm at 488 nm, based on the equation:

$$\delta\lambda_{min} = \Delta\lambda/\Delta r \times \text{FWHM}_{\text{focal spot}} \tag{7}$$

where $\delta\lambda_{min}$ is the minimum resolvable wavelength difference (i.e., the spectral resolution of the spectrometer) and the

FWHM ($\text{FWHM}_{\text{focal spot}}$) is 58 µm, as determined from experimental measurements (Figure 3a).[25] This is the result based on the intrinsic properties of the metalens alone. To take into account the pixel size of the camera, Equation (7) has to be modified:

$$\delta\lambda_{min} = \frac{\Delta\lambda}{\Delta r} \times \text{FWHM}_{\text{focal spot}} + \frac{\Delta\lambda}{\Delta r} \times 3D \tag{8}$$

where D is the pixel size of the camera.[26] This yields a final, combined resolution of about 1 nm. In other words, by using a low numerical aperture, aberration-corrected metalens with a working distance of 4 cm to the detector, we can achieve nanometer spectral resolution across 200 nm in the visible. Applying Equation (8) to the results from Figure 3, we find a spectral resolution of 0.96, 1.01, 1.06, and 1.14 nm at 488, 532, 632, and 660 nm incident wavelengths, respectively. We have
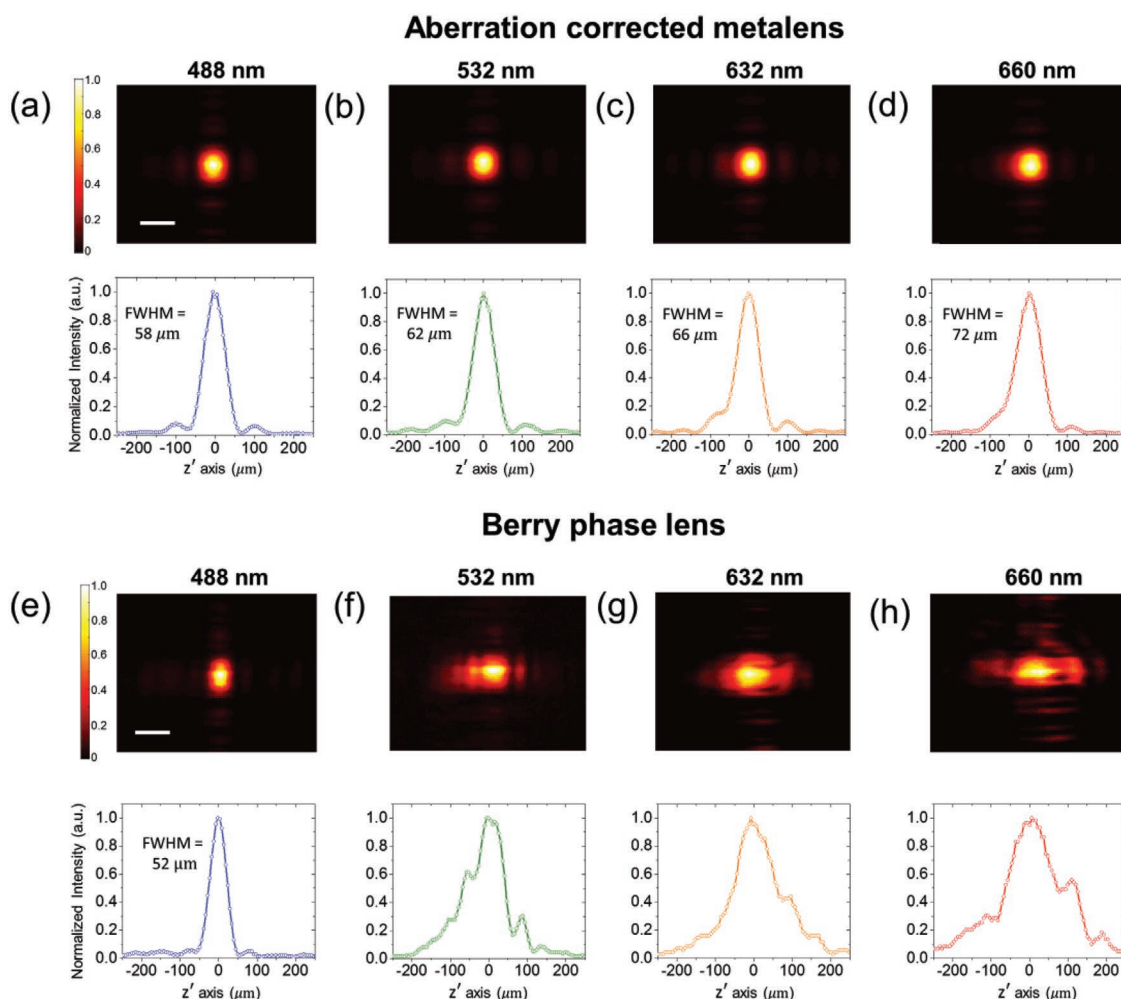
Aberration corrected metalens

Berry phase lens

Figure 3. Experimental characterization of the focal spots and their respective (normalized) intensity cross-sections of a–d) the aberration-corrected metalens, and e–h) the Berry phase lens used as a control under monochromatic laser illumination at 488, 532, 632, and 660 nm. Both lenses were fabricated on the same sample and the data were measured simultaneously using a single camera. Scale bars: 100 μm

also included the calculated spectral resolution across the entire bandwidth of interest and present it in the Supporting Information (Figure S3, Supporting Information).

The efficiency of the metalens as a function of wavelength is defined as the power contained in the focal spot, normalized to the incident power passing through an aperture with the
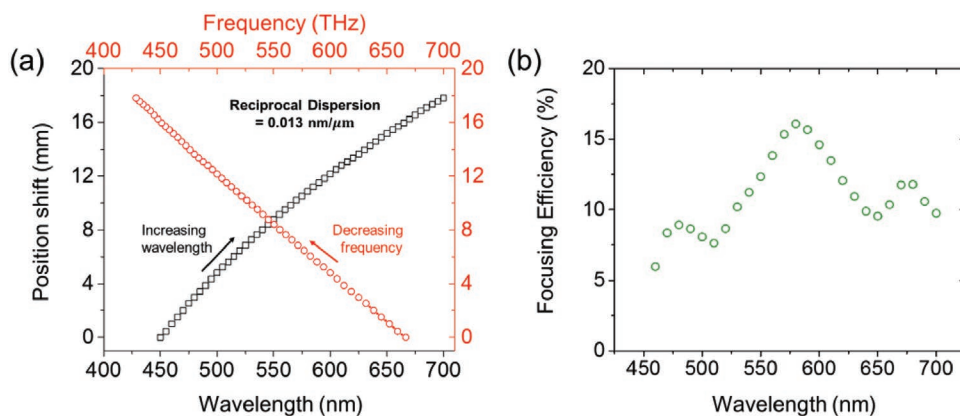

Figure 4. a) Dispersion of the aberration-corrected metalens plotted as a function of both wavelength (black) and frequency (red). Note that although the dispersion appears to be approximately linear in frequency, it is not rigorously so, based on Equations (1)–(6). b) Focusing efficiency of the aberration-corrected metalens.

ADVANCED
SCIENCE NEWS
www.advancedsciencenews.com

ADVANCED
OPTICAL
MATERIALS
www.advopticalmat.de

same size as the lens (800 × 250 µm) and the glass substrate. These values are generally low (<15% in Figure 4b), partly due to the lack of degrees of freedom in the coupled nano-fin elements to independently optimize for efficiency, in addition to implementing the phase, GD and GDD profiles. Implementing an accurate phase and dispersion profile is our priority since this dictates the resolution and performance of the lens. This results in a situation where different nanofins across the lens may have extremely different efficiencies due to the design algorithm. Consequently, to avoid excessive amplitude modulation which introduces spurious, unwanted diffraction orders, we chose the elements with nearly uniform amplitude across the design bandwidth, at the cost of overall efficiency. This problem can be mitigated by adopting more complicated structures than coupled nanofins, which would provide more degrees of freedom during design and optimization.[36,37] We also attribute the loss in efficiency to a slightly reduced accuracy of fitting the phase profile (due to the requirement of fitting higher order terms), as well as fabrication imperfections.

3. Metasurface as Aberration Corrector

Beyond a highly compact spectrometer with nanometer resolution across a broad bandwidth, some applications also call for customized dispersion characteristics. For example, in Raman spectroscopy a linear dispersion in the frequency domain is sometimes desired to simplify calibration procedures and minimize error. Although the current dispersion of the aberration-corrected metalens spectrometer appears to be almost linear in frequency (Figure 4a), it is not rigorously so. This is apparent upon inspection of Equation (3): the derivative of z (spatial coordinate of the focal spot) with respect to frequency is not a constant. A straightforward way to proceed is to rewrite both the focal length and focusing angle of the metalens such that the derivative of the focal spot z-coordinate $z = f(\omega) \cdot \cos(\theta(\omega))$ with respect to frequency is now a constant, while ensuring that the focal spots for different wavelengths remain along a plane. However, this would require a completely new phase profile (Equation (1)) and the required GD and GDDs would be very large (up to 1000s of femtoseconds squared), which would be almost impossible to realize in a real device. A similar challenge exists for the design of spatially large metalenses with high numerical aperture.

Figure 5a shows one way to overcome this challenge: by inserting an additional correcting metasurface, one can maintain the metalens phase profile while introducing comparatively small changes to the GD and GDD to slightly perturb $f(\omega)$ and $\theta(\omega)$, such that the focal spot position along the focal plane is strictly linear with respect to frequency. In practice, this can be a doublet or simply another metasurface placed in free space, as long as the distance between the two components is taken into account during the design step.

The calculated focal length shift of such a doublet is plotted together with our previous result for the singlet aberration-corrected metalens in Figure 5b. Although the curves are closely spaced, which is expected since the original dispersion is approximately linear (Figure 4a), some corrections to the focal spot positions are introduced by the doublet such that the final dispersion (orange line in Figure 5b) becomes strictly linear. By design, we require the focal spot positions at the beginning and end of the operating spectral range of the doublet to be identical to the singlet (blue line in Figure 5b): this would ensure that only the intermediate focal spot positions are being corrected for, which translates into minimal GD and GDD required for the additional metasurface corrector. The phase profiles of the metasurface corrector for various wavelengths were determined by using optimization tools in the ray-tracing software Zemax OpticStudio. Figure 5c plots the required phase (along the x-axis) at the edge of this metasurface as a function of frequency. Note that at the extremes of the spectral range of interest, the required phase is approximately equal since we wish to retain the original focal spot positions of the singlet metalens. The orange crosses and black circles in Figure 5c correspond to second and third-order polynomial fits to this target phase, respectively; these fitting coefficients in turn define the values of GD and GDD needed to implement the phase profile. Within our current library of elements, we are only able to reliably engineer up to second-order terms (GDD), resulting in some small but nonzero phase error. However, in our lens design methodology, we are usually able to limit the resulting wavefront error to less than 0.075λ (the Maréchal criterion) such that the focal spot is still diffraction limited.

A representative sample of GD and GDD values needed for the metasurface corrector is plotted in Figure 5d. Each point represents an element which was chosen to satisfy the target phase profile across the spectral range of interest. Note that the range of GD and GDD values needed are approximately 5 fs and 140 fs^2, respectively. Based on our existing library of nanostructures used in this work and others[17] which have GD and GDD ranges of 5 fs and 10 fs^2, we believe that these requirements can be met using nanofabrication technologies,[38] or by using a hybrid lens comprising of both diffractive and dispersion-engineered metasurface elements. Additionally, in the metasurface corrector the dispersion engineering primarily takes place along the x-axis; this is similar to the original design of the aberration-corrected metalens where the choice of the focal plane (parallel to the z-axis) ensures that minimal dispersion is needed along y (inset of Figure 5d).

We note that by incorporating third-order corrections (see Figure S4, Supporting Information) to the phase, one would be able to fit the target phase profile more accurately and eliminate the small phase errors mentioned previously. This would ensure diffraction-limited focusing across the entire spectrum of interest, and can be accomplished by introducing additional degrees of freedom to the nanostructures.

In the current design, we have made use of anisotropic nanostructures for the metalens. Consequently, the spectrometer works only for one helicity of circularly polarized light. For applications where polarization insensitivity is crucial, one can use instead isotropic nanostructures such as pillars or squares.[39–41] A similar approach of using more complicated shapes would be necessary for the angular dispersion engineering[42–44] of other devices such as Fourier or
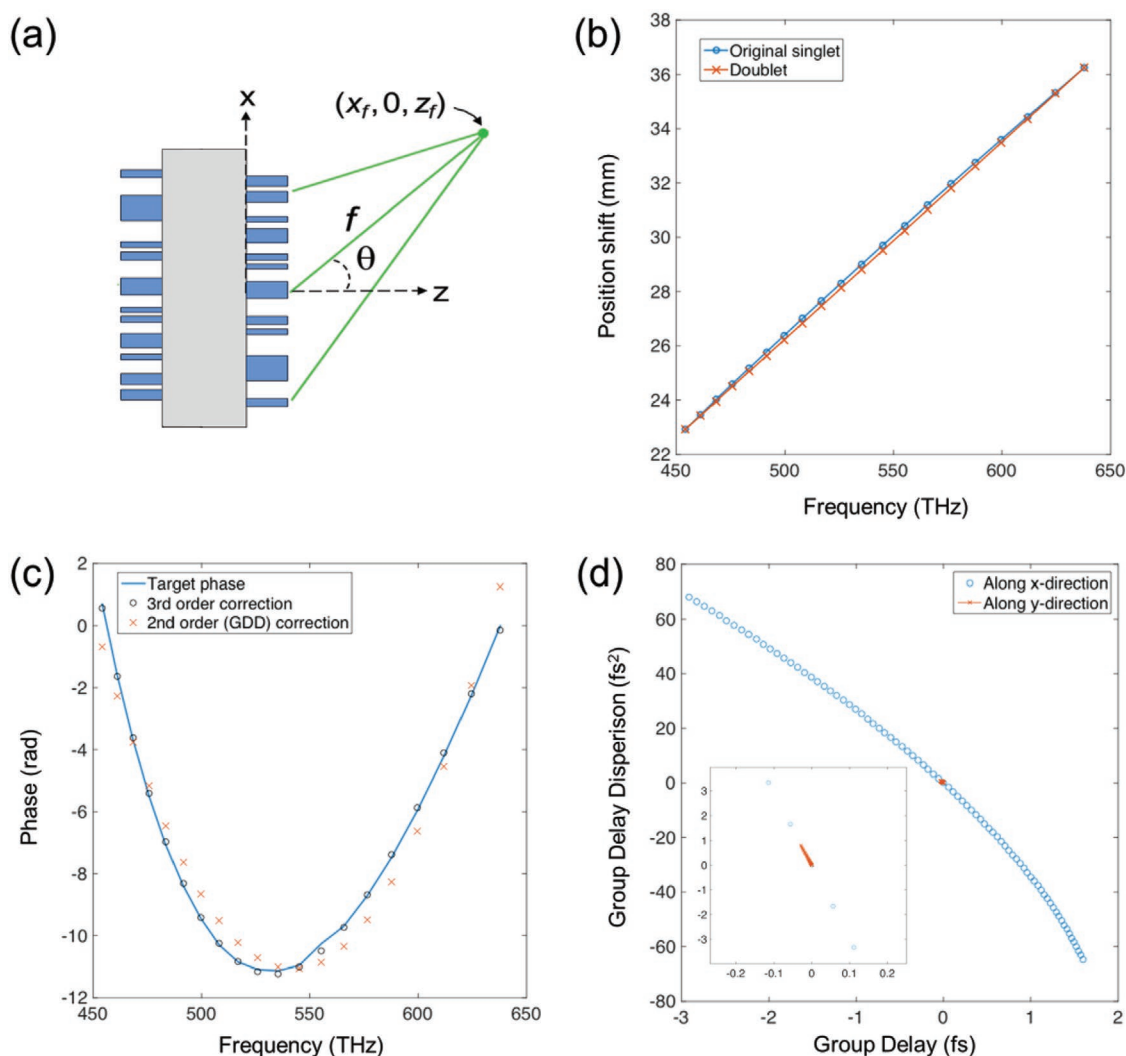
**ADVANCED
SCIENCE NEWS**
www.advancedsciencenews.com

**ADVANCED
OPTICAL
MATERIALS**
www.advopticalmat.de

Figure 5. a) Schematic of a doublet, comprising of a metasurface corrector and the original aberration-corrected off-axis metalens. The corrector serves to impart GD and GDDs such that the focal spot positions of the metalens are linear in frequency. b) Plots of the focal spot positions of the singlet metalens (blue) and the doublet (orange) as a function of frequency. c) Plot of the required phase as a function of frequency for an element at the edge of the metasurface corrector (blue line), and the results of second- and third-order polynomial fits (orange crosses and black circles, respectively). d) GD and GDD values required for elements across the middle of the metasurface corrector, along x and y directions (blue circles and orange crosses). Inset: magnified view of the dispersion required for elements along y, which is minimal, due to the choice of the orthogonal camera plane.

subresolution metalenses.[45–47] Another intriguing possibility is the use of topology optimization to design freeform shapes with these desired functionalities.[37]

We would also like to comment on the related problem of expanding the spectral range of the device to the ultraviolet and infrared regimes. From a design perspective, this necessitates the correction of even higher orders of dispersion (e.g., third- and even fourth-order derivatives of phase with respect of frequency). While this might be prohibitive for a single metalens due to design complexity, this is possible by the same technique of using a metacorrector in conjunction with a refractive or diffractive optics lens, as discussed previously. From a practical point of view, this would require the nanofabrication of materials with a very large bandgap which would remain low-loss in the ultraviolet region, such as transition metal fluorides, fused silica, and nitrides.[48,49]

4. Conclusion

In summary, we have demonstrated an aberration-corrected off-axis metalens which allows us to realize a highly compact spectrometer with nanometer resolution across 200 nm in the visible. This was made possible by engineering the dispersion of the metalens, i.e., higher order derivatives of phase with respect to frequency, using coupled nanofin elements. This approach can correct for chromatically induced astigmatism and field curvature in metalens spectrometers and essentially engineer the focal length to be an arbitrary function of frequency. We highlighted one example of using a metalens doublet to achieve strictly linear dispersions in frequency; similar applications are limited only by the range of GD or GDDs the nanostructures can provide, which are in turn determined by fabrication technologies. We believe that this technology can

lead to exciting advances and applications not just in spectroscopy, but also consumer/wearable optics products in general.

[1] D. A. Long, *Raman Spectroscopy*, McGraw-Hill, New York **1977**.
[2] J. R. Lakowicz, *Fluorescence Studies on Biological Membranes*, Springer, New York **1988**.
[3] R. S. Lunetta, C. D. Elvidge, *Remote Sensing Change Detection*, Taylor & Francis, United Kingdom **1999**.
[4] W. Wang, J. Paliwal, *Sens. Instrum. Food Quality Safety* **2007**, *1*, 193.
[5] A. Schuurs, B. Van Weemen, *Clin. Chim. Acta* **1977**, *81*, 1.
[6] A. Y. Zhu, F. Yi, J. C. Reed, H. Zhu, E. Cubukcu, *Nano Lett.* **2014**, *14*, 5641.
[7] M. Czerny, A. Turner, *Z. Phys.* **1930**, *61*, 792.
[8] Q. Xue, *Appl. Opt.* **2011**, *50*, 1338.
[9] T. Kita, T. Harada, N. Nakano, H. Kuroda, *Appl. Opt.* **1983**, *22*, 512.
[10] J. Reimers, A. Bauer, K. P. Thompson, J. P. Rolland, *Light: Sci. Appl.* **2017**, *6*, e17026.
[11] F. Capasso, *Nanophotonics* **2018**, *7*, 953.
[12] F. Monticone, N. M. Estakhri, A. Alù, *Phys. Rev. Lett.* **2013**, *110*, 203903.
[13] N. Yu, F. Capasso, *Nat. Mater.* **2014**, *13*, 139.
[14] A. Arbabi, Y. Horie, M. Bagheri, A. Faraon, *Nat. Nanotechnol.* **2015**, *10*, 937.
[15] D. Lin, P. Fan, E. Hasman, M. L. Brongersma, *Science* **2014**, *345*, 298.
[16] M. Khorasaninejad, W. T. Chen, R. C. Devlin, J. Oh, A. Y. Zhu, F. Capasso, *Science* **2016**, *352*, 1190.
[17] W. T. Chen, A. Y. Zhu, V. Sanjeev, M. Khorasaninejad, Z. Shi, E. Lee, F. Capasso, *Nat. Nanotechnol.* **2018**, *13*, 220.
[18] P. R. West, J. L. Stewart, A. V. Kildishev, V. M. Shalaev, V. V. Shkunov, F. Strohkendl, Y. A. Zakharenkov, R. K. Dodds, R. Byren, *Opt. Express* **2014**, *22*, 26212.
[19] G. Zheng, H. Mühlenbernd, M. Kenney, G. Li, T. Zentgraf, S. Zhang, *Nat. Nanotechnol.* **2015**, *10*, 308.
[20] X. Li, L. Chen, Y. Li, X. Zhang, M. Pu, Z. Zhao, X. Ma, Y. Wang, M. Hong, X. Luo, *Sci. Adv.* **2016**, *2*, e1601102.
[21] X. Ni, A. V. Kildishev, V. M. Shalaev, *Nat. Commun.* **2013**, *4*, 2807.
[22] W. T. Chen, P. Török, M. R. Foreman, C. Y. Liao, W.-Y. Tsai, P. R. Wu, D. P. Tsai, *Nanotechnology* **2016**, *27*, 224002.
[23] J. B. Mueller, K. Leosson, F. Capasso, *Optica* **2016**, *3*, 42.
[24] A. Pors, M. G. Nielsen, S. I. Bozhevolnyi, *Optica* **2015**, *2*, 716.
[25] A. Y. Zhu, W.-T. Chen, M. Khorasaninejad, J. Oh, A. Zaidi, I. Mishra, R. C. Devlin, F. Capasso, *APL Photonics* **2017**, *2*, 036103.
[26] M. Khorasaninejad, W. T. Chen, J. Oh, F. Capasso, *Nano Lett.* **2016**, *16*, 3732.
[27] C. Zhang, G. Cheng, P. Edwards, M.-D. Zhou, S. Zheng, Z. Liu, *Lab Chip* **2016**, *16*, 246.
[28] N. Savage, *Nat. Photonics* **2009**, *3*, 601.
[29] P. Gatkine, S. Veilleux, Y. Hu, J. Bland-Hawthorn, M. Dagenais, *Opt. Express* **2017**, *25*, 17918.
[30] M. Faraji-Dana, E. Arbabi, A. Arbabi, S. M. Kamali, H. Kwon, A. Faraon, *Nat. Commun.* **2018**, *9*, 4196.
[31] M. Murty, *Opt. Eng.* **1974**, *13*, 130123.
[32] R. C. Devlin, M. Khorasaninejad, W. T. Chen, J. Oh, F. Capasso, *Proc. Natl. Acad. Sci. USA* **2016**, *113*, 10473.
[33] M. V. Berry, *J. Mod. Opt.* **1987**, *34*, 1401.
[34] S. Pancharatnam, *Proc. Indian Acad. Sci. - Sec. A* **1956**, *44*, 398.
[35] V. R. Almeida, Q. Xu, C. A. Barrios, M. Lipson, *Opt. Lett.* **2004**, *29*, 1209.
[36] D. Sell, J. Yang, E. W. Wang, T. Phan, S. Doshay, J. A. Fan, *ACS Photonics* **2018**, *5*, 2402.
[37] Z. Lin, B. Groever, F. Capasso, A. W. Rodriguez, M. Lončar, *Phys. Rev. Appl.* **2018**, *9*, 044030.
[38] S. Lee, B. Park, J. S. Kim, T.-i. Kim, *Nanotechnology* **2016**, *27*, 474001.
[39] M. Khorasaninejad, A. Y. Zhu, C. Roques-Carmes, W. T. Chen, J. Oh, I. Mishra, R. C. Devlin, F. Capasso, *Nano Lett.* **2016**, *16*, 7229.
[40] M. Khorasaninejad, Z. Shi, A. Y. Zhu, W.-T. Chen, V. Sanjeev, A. Zaidi, F. Capasso, *Nano Lett.* **2017**, *17*, 1819.
[41] S. Shrestha, A. Overvig, M. Lu, A. Stein, N. Yu, *Light Sci. Appl.* **2018**, *7*, 85.
[42] S. M. Kamali, E. Arbabi, A. Arbabi, Y. Horie, M. Faraji-Dana, A. Faraon, *Phys. Rev. X* **2017**, *7*, 041056.
[43] A. Akbarzadeh, N. Chamanara, C. Caloz, *Opt. Lett.* **2018**, *43*, 3297.
[44] M. Qiu, M. Jia, S. Ma, S. Sun, Q. He, L. Zhou, *Phys. Rev. Appl.* **2018**, *9*, 054050.
[45] W. Liu, Z. Li, H. Cheng, C. Tang, J. Li, S. Zhang, S. Chen, J. Tian, *Adv. Mater.* **2018**, *30*, 1706368.
[46] R. Zuo, W. Liu, H. Cheng, S. Chen, J. Tian, *Adv. Opt. Mater.* **2018**, *6*, 1800795.
[47] E. T. Rogers, J. Lindberg, T. Roy, S. Savo, J. E. Chad, M. R. Dennis, N. I. Zheludev, *Nat. Mater.* **2012**, *11*, 432.
[48] S. Colburn, A. Zhan, E. Bayati, J. Whitehead, A. Ryou, L. Huang, A. Majumdar, *Opt. Mater. Express* **2018**, *8*, 2330.
[49] B. H. Chen, P. C. Wu, V.-C. Su, Y.-C. Lai, C. H. Chu, I. C. Lee, J.-W. Chen, Y. H. Chen, Y.-C. Lan, C.-H. Kuan, *Nano Lett.* **2017**, *17*, 6345.